

Lorentz violation in nucleon electromagnetic moments

Javier Montaña-Domínguez

Cátedras Conacyt-Facultad de Ciencias Físico Matemáticas, Universidad Michoacana de San Nicolás de Hidalgo, Av. Francisco J. Múgica s/n, C. P. 58060, Morelia, Michoacán, México.

Héctor Novales-Sánchez*, Mónica Salinas, J. Jesús Toscano

Facultad de Ciencias Físico Matemáticas, Benemérita Universidad Autónoma de Puebla, Apartado Postal 1152 Puebla, Puebla, México

Abstract

Yukawa couplings from the Lorentz- and CPT -violating Standard Model Extension induce quantum contributions to the magnetic and electric moments of quarks, which are calculated in the present paper. Then we take advantage of the high sensitivity measurements of the proton and neutron electromagnetic moments (EMM), suitable to search for tiny effects of new physics, to constrain coefficients parametrizing Lorentz violation, reaching bounds as restrictive as 10^{-23} .

Keywords: Lorentz violation, electromagnetic properties of quarks

The Lorentz and CPT -violating Standard Model Extension (SME) [1, 2], built upon the generality provided by effective theories, is a valuable tool for phenomenologists to look for traces, even if tiny, of effects produced by the breaking of Lorentz invariance [3, 4, 5, 6]. A plethora of papers has been dedicated to bound SME coefficients [7], among the huge list of parameters characterizing the sectors for this effective-Lagrangian description. The present work provides a calculation of contributions from the renormalizable-SME Yukawa sector [2, 8] to the anomalous magnetic moment (AMM) and to the electric dipole moment

*Corresponding author

Email address: `hector.novales@correo.buap.mx` (Héctor Novales-Sánchez*)

(EDM) of quarks, as well as an estimation of SME coefficients of this sector, in accordance with current bounds on the neutron and the proton EMM [9, 10, 11].

The quark Yukawa sector of the renormalizable SME, $\mathcal{L}_{Y,q}^{\text{SME}}$, involves the $\text{SU}(2)_L$ spinor doublets Q_A and singlets u'_A, d'_A , with $A = u, c, t$, and the Higgs doublet, ϕ , as well. These fields couple through Yukawa-like constants $(H_u)_{\mu\nu}^{AB}$ and $(H_d)_{\mu\nu}^{AB}$, invariant under particle Lorentz transformations [1, 2] and bearing both quark-flavor indices A, B and spacetime indices μ, ν . Implementation of chiral unitary transformations U_L^f and U_R^f , after spontaneous breaking of the electroweak symmetry, then yields [8]

$$\begin{aligned}\mathcal{L}_{Y,q}^{\text{SME}} &= -\frac{1}{2}(H_u)_{\mu\nu}^{AB}\overline{Q}_A\tilde{\phi}\sigma^{\mu\nu}u'_B - \frac{1}{2}(H_d)_{\mu\nu}^{AB}\overline{Q}_A\phi\sigma^{\mu\nu}d'_B + \text{H.c.} \\ &= -\frac{1}{2}(v+H)\sum_{f=u,d}\overline{f}_A\left((V_f)_{\mu\nu}^{AB}+(A_f)_{\mu\nu}^{BA*}\gamma_5\right)\sigma^{\mu\nu}f_B,\end{aligned}\quad (1)$$

where $(V_f)_{\mu\nu}^{AB} = \frac{1}{2}((Y_f)_{\mu\nu}^{AB} + (Y_f)_{\mu\nu}^{BA*})$ and $(A_f)_{\mu\nu}^{AB} = \frac{1}{2}((Y_f)_{\mu\nu}^{AB} - (Y_f)_{\mu\nu}^{BA*})$, with $(Y_f)_{\mu\nu} = U_L^{f\dagger}(H_f)_{\mu\nu}U_R^f$. Flavor-space 3×3 matrices $(V_f)_{\mu\nu}$ and $(A_f)_{\mu\nu}$ are Hermitian and antiHermitian, respectively, whereas spacetime-group 4×4 matrices $(V_f)^{AB}$ and $(A_f)^{AB}$ are both antisymmetric. Note that, at this stage, quark-flavor indices A, B run over either u, c, t or d, s, b , depending on whether $f = u$ or $f = d$.

There are one-loop contributions to the electromagnetic vertex $A_\mu f_A f_A$ from Feynman diagrams with 2-point and/or 3-point Lorentz-violating insertions, derived from Eq. (1). Contributions from the SME Yukawa sector to AMMs and EDMs emerge for the first time at the second order in Lorentz-violating coefficients $(V_f)_{\mu\nu}^{AB}$ and $(A_f)_{\mu\nu}^{AB}$ [12]. The corresponding amplitude reads

$$\sum_B \left(\text{diagram 1} + \text{diagram 2} + \text{diagram 3} \right) + \dots = \overline{\mathcal{U}}_A \left(\frac{ef_A^{\text{M}}}{2m_A} + if_A^{\text{E}}\gamma_5 \right) \sigma_{\mu\nu} q^\nu \mathcal{U}_A + \dots, \quad (2)$$

where \mathcal{U}_A is a momentum-space quark spinor, and q denotes the incoming momentum of the external photon. Moreover, $f_A^{\text{M}}(q^2)$ and $f_A^{\text{E}}(q^2)$ define the AMM and the EDM by $a_A = f_A^{\text{M}}(q^2 = 0)$ and $d_A = f_A^{\text{E}}(q^2 = 0)$, respectively [13, 14],

with both quantities preserving Lorentz invariance. Those diagrams explicitly displayed in the left-hand side of Eq. (2) produce the leading contributions, while the presence of other diagrams has been indicated by the ellipsis. Dots on internal lines of such diagrams represent 2-point insertions, which either preserve or change quark flavor, so $B = A$ or $B \neq A$, with all the corresponding diagrams summed together in Eq. (2).

In the space of matrix representations of Lorentz transformations, the matrices $(\kappa_1^{AB})_\mu{}^\nu = V_{\mu\rho}^{AB} V^{AB\rho\nu}$, $(\kappa_2^{AB})_\mu{}^\nu = A_{\mu\rho}^{BA*} A^{BA\rho\nu*}$, and $(\kappa_3^{AB})_\mu{}^\nu = V_{\mu\rho}^{AB} A^{BA\rho\nu*}$ are defined, comprising 324 parameters. Following Ref. [12], we define the 3×3 matrices χ_j , with $j = 1, 2, 3$, through their entries: $\chi_j^{AB} = \text{tr } \kappa_j^{AB}$. The SME Yukawa-sector contributions to AMMs and EDMs are then written as $a_A^{\text{SME}} = \sum_{j=1}^2 \sum_B a_j^{AB} \chi_j^{AB}$, and $d_A^{\text{SME}} = \sum_B d_3^{AB} \chi_3^{AB}$. We find ultraviolet-finite results, though infrared divergencies remain. As argued in Ref [12], such divergences are expected to vanish from cross sections, so we disregard them throughout our forthcoming discussion. Note, however, that these AMMs and EDMs are not to be understood as observables, while they can provide us with estimations of the impact of Lorentz violation on physical processes involving the quark electromagnetic vertex. In general, the AMM and EDM contributions are complex quantities, even though all the external lines have been taken on shell. This occurs as long as perturbative 2-point insertions connect external lines to virtual lines of lighter particles, since this induces thresholds [12]. The only exceptions are the EMM of the up and down quarks, as in such cases external particles are always lighter than virtual particles, which then yields real-valued contributions.

We consider a scenario of *quasidiagonal textures* (QDT), defined by the condition $\chi_j^{AB} \approx 0$ for $A \neq B$, so we write the SME contributions to the AMMs and EDMs of the proton, p , and neutron, n , as

$$a_N^{\text{SME}} = \sum_{f=u,d} \xi_N^f (a_1^{ff} \Delta_f + a_2^{ff}) \chi_2^{ff}, \quad d_N^{\text{SME}} = \sum_{f=u,d} \xi_N^f d_j^{ff} \chi_3^{ff}, \quad (3)$$

where $N = p, n$, $\xi_p^u = 4/3$, $\xi_p^d = -1/3$, $\xi_n^u = -1/3$, and $\xi_n^d = 4/3$. Furthermore, the factors $\Delta_f = \frac{\chi_1^{ff}}{\chi_2^{ff}}$, with $f = u, d$, have been defined. Note that χ_1^{ff} and χ_2^{ff} are real, whereas χ_3^{ff} is imaginary. Fig. 1 displays allowed regions for SME coefficients χ_2^{ff} and $-i\chi_3^{ff}$, as implied by current bounds on the EMM of these nucleons [9, 10, 11]. The magnetic moments of the proton and the neutron

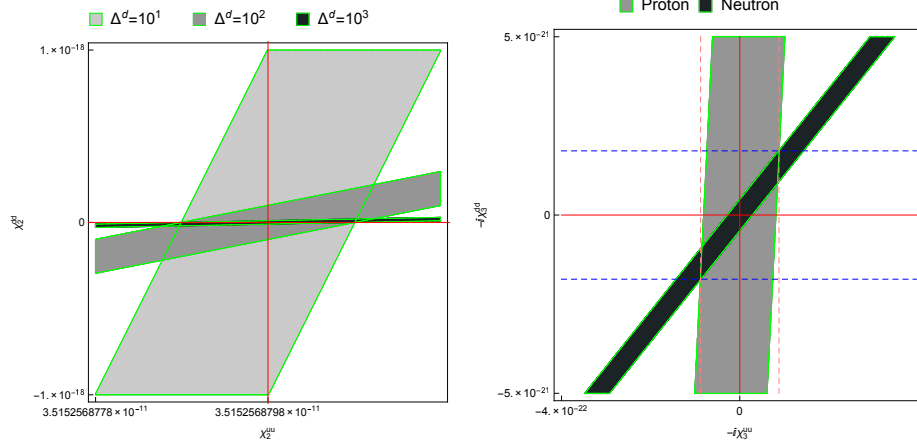


Figure 1: Allowed regions in the scenario of QDT matrices χ_j . Left-hand graph: the parameter space $(\chi_2^{uu}, \chi_2^{dd})$, from the limit on the magnetic moment of the proton. Right-hand graph: the parameter space $(-i\chi_3^{uu}, -i\chi_3^{dd})$, from the EDMs of both the proton and the neutron.

have been reported to be $\mu_p = 2.7928473446(8)\mu_N$ and $\mu_n = -1.9130427(5)\mu_N$, respectively, with μ_N the nuclear magneton. By assuming that new-physics traces might be as large as the errors in these data, the proton magnetic moment measurement, better than the one for the neutron by three orders of magnitude, is our choice to constrain SME coefficients. Relying on this bound, the first graph in Fig. 1 shows allowed regions in the parameter space $(\chi_2^{uu}, \chi_2^{dd})$, within $|\chi_2^{dd}| < 10^{-18}$ and $\chi_2^{uu} = 3.5152568798(20) \times 10^{-11}$, which correspond to fixed $\Delta_u = 10^1$, with $\Delta_d = 10^1$ (light gray), 10^2 (dark gray), 10^3 (black). Since allowed regions are straight bands, there exist only one subset of the parameter space, displayed in the graph, in which they intersect. Clearly, the larger the factor Δ_d the more stringent the restrictions on χ_2^{dd} . Regarding the EDMs of the nucleons, current bounds are $|d_p| < 0.021 \times 10^{-23}e\text{ cm}$ and

$|d_n| < 0.18 \times 10^{-25} e \text{ cm}$. The second graph in Fig. 1 provides allowed regions in accordance with both limits. The gray region comes from the proton EDM bound, whereas the black region is defined by measurement of the neutron EDM. As expected, the neutron EDM yields the most strict restrictions on the SME coefficients χ_3^{ff} . Nevertheless, it is the intersection of the two regions the one which defines the allowed values for the SME coefficients. All the bounds from the present analysis are given in Table 1.

Assumptions	EMM	LVP	Bounds
QDT, $\Delta_d = 10^1$, $\Delta_u = 10^1$	a_p^{SME}	χ_2^{uu}	$3.5152568798(20) \times 10^{-11}$
		$ \chi_2^{dd} $	$< 10^{-18}$
QDT, $\Delta_d = 10^1$, $\Delta_u = 10^2$	a_p^{SME}	χ_2^{uu}	$3.5152568798(20) \times 10^{-11}$
		χ_2^{dd}	$(-0.0004 \pm 2.9527) \times 10^{-19}$
QDT, $\Delta_d = 10^1$, $\Delta_u = 10^3$	a_p^{SME}	χ_2^{uu}	$3.5152568798(20) \times 10^{-11}$
		χ_2^{dd}	$(-0.0004 \pm 2.9473) \times 10^{-20}$
QDT	$d_p^{\text{SME}}, d_n^{\text{SME}}$	$ \chi_3^{uu} $	$< 8.8 \times 10^{-23}$
		$ \chi_3^{dd} $	$< 1.8 \times 10^{-21}$
HYM	a_p^{SME}	χ_1^{uu}	$(-0.21 \pm 2.99) \times 10^{-19}$
		χ_1^{ut}	$-3.7837161472(22) \times 10^{-12}$
HYM, $\Omega_d = 10^1$	a_p^{SME}	χ_1^{dd}	$(-0.03 \pm 0.98) \times 10^{-16}$
		χ_1^{ds}	$7.88744831(2) \times 10^{-7}$
HYM, $\Omega_d = 10^2$	a_p^{SME}	χ_1^{dd}	$(-0.037 \pm 1.076) \times 10^{-16}$
		χ_1^{ds}	$7.88744831(2) \times 10^{-7}$
HYM, $\Omega_d = 10^3$	a_p^{SME}	χ_1^{dd}	$(-0.037 \pm 1.076) \times 10^{-16}$
		χ_1^{ds}	$7.8874483107(31) \times 10^{-7}$

Table 1: Bounds on Lorentz-violation parameters (LVP) of the renormalizable-SME Yukawa sector.

Another scenario is that of *Hermitian Y matrices* (HYM), in which case all contributions to EDMs vanish, whereas $\chi_2 = 0$ as well, thus leaving only χ_1

nonzero. The proton AMM reads $a_p^{\text{SME}} = \sum_f \sum_A \xi_p^f a_1^{fA} \chi_1^{fA}$, with $f = u, d$ and the quark-flavor index A running over either $A = u, c, t$, if $f = u$ or $A = d, s, b$, whenever $f = d$. Assuming that fine tuning is absent, we estimate and analyze the up- and down-quark contributions to the proton AMM, $a_{p,u}^{\text{SME}}$ and $a_{p,d}^{\text{SME}}$, separately. We write the contributions as

$$a_{p,u}^{\text{SME}} \approx \xi_p^u (a_1^{ut} \chi_1^{ut} + a_1^{uu} \chi_1^{uu}), \quad a_{p,d}^{\text{SME}} = \xi_p^d ((\Omega_d a_1^{db} + a_1^{dd}) \chi_1^{dd} + a_1^{ds} \chi_1^{ds}), \quad (4)$$

where $\Omega_d = \frac{\chi_1^{db}}{\chi_1^{da}}$. A term $\xi_p^u a_1^{uc} \chi_1^{uc}$ has been neglected from the left-hand expression of Eq. (4) as both $a_1^{uc} \ll a_1^{ut}$ and $a_1^{uc} \ll a_1^{uu}$ hold. Allowed regions in the parameter spaces $(\chi_1^{uu}, \chi_1^{ut})$ and $(\chi_1^{ds}, \chi_1^{dd})$, established by the proton magnetic moment bound, are displayed in Fig. (2). The first graph of this figure, plot-

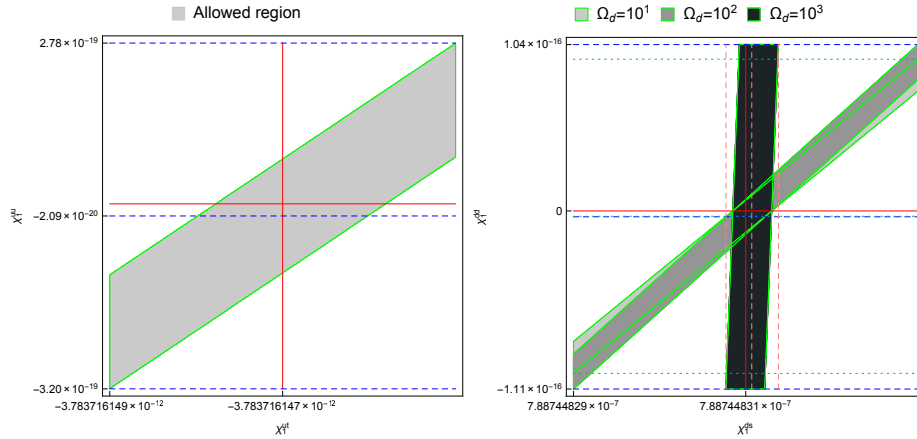


Figure 2: Allowed regions in the scenario of χ_j from HYM, determined from the bound on the proton magnetic moment. Left-hand graph: the parameter space $(\chi_1^{ut}, \chi_1^{uu})$. Right-hand graph: the parameter space $(\chi_1^{ds}, \chi_1^{dd})$.

ted in the parameter space $(\chi_1^{uu}, \chi_1^{ut})$, has been carried out for values within intervals $\chi_1^{uu} = (-0.21 \pm 2.99) \times 10^{-19}$ and $\chi_1^{ut} = -3.7837161472(22)$. The solid horizontal line represents the value $\chi_1^{uu} = 0$, whereas $\chi_1^{ut} = -3.783716147$ defines the vertical solid line in this graph. Three dashed horizontal lines, associated to $\chi_1^{uu} = 2.78 \times 10^{-19}$, -2.09×10^{-20} , -3.20×10^{-19} , have been included as well. On the other hand, the second graph of Fig. 2 displays three different regions, corresponding to $\Omega_d = 10^1, 10^2, 10^3$. All these allowed regions, which

are bands, have been carried out to show the only subregion of the parameter space $(\chi_1^{ds}, \chi_1^{dd})$ in which they intersect. As larger values of Ω_d are considered, the corresponding allowed region is rotated counterclockwise, meanwhile it becomes wider. Again, bounds derived from this analysis are illustrated in Table 1.

In the present work the contributions from the renormalizable-SME Yukawa sector to the EMM of quarks have been calculated. Following the standard prescription to connect the EMM of the up and down quarks to those of the nucleons, our results have been utilized to estimate contributions to AMMs and EDMs of the proton and the neutron, whose comparison with current bounds have yielded constraints on SME coefficients which parametrize effects of Lorentz violation at low energies. Bounds as stringent as 10^{-23} have been established.

Acknowledgements

We acknowledge financial support from CONACYT and SNI (México).

References

- [1] D. Colladay and V. A. Kostelecký, *CPT* violation and the standard model, Phys. Rev. D **55**, (1997) 6760.
- [2] D. Colladay and V. A. Kostelecký, Lorentz-violating extension of the standard model, Phys. Rev. D **58** (1998) 116002.
- [3] V. A. Kostelecký and S. Samuel, Spontaneous breaking of Lorentz symmetry in string theory, Phys. Rev. D **39** (1989) 683.
- [4] V. A. Kostelecký and R. Potting, CPT and strings, Nucl. Phys. B **359** (1991) 545.
- [5] V. A. Kostelecký and R. Potting, CPT, strings, and meson factories, Phys. Rev. D **51** (1995) 3923.

- [6] S. M. Carroll, J. A. Harvey, V. A. Kostelecký, C. D. Lane, and T. Okamoto, Noncommutative Field Theory and Lorentz Violation, *Phys. Rev. Lett.* **87** (2001) 141601.
- [7] V. A. Kostelecký and N. Russell, Data tables for Lorentz and *CPT* violation, *Rev. Mod. Phys.* **83** (2011) 11.
- [8] A. I. Hernández-Juárez, J. Montaña, H. Novales-Sánchez, M. Salinas, J. Toscano, and O. Vázquez-Hernández, One-loop structure of the photon propagator in the standard model extension, *Phys. Rev. D* **99** (2019) 013002.
- [9] G. Schneider *et al.*, Double-trap measurement of the proton magnetic moment at 0.3 parts per billion precision, *Science* **358** (2017) 1081.
- [10] J. M. Pendlebury *et al.*, Revised experimental upper limit on the electric dipole moment of the neutron, *Phys. Rev. D* **92** (2015) 092003.
- [11] P.A. Zyla *et al.* (Particle Data Group), Review of particle physics, *Prog. Theor. Exp. Phys.* **2020** (2020) 083C01.
- [12] J. A. Ahuatzzi-Avendaño, J. Montaña, H. Novales-Sánchez, M. Salinas, and J. J. Toscano, Bounds on Lorentz-violating Yukawa couplings via lepton electromagnetic moments, *Phys. Rev. D* **103** (2021) 055003.
- [13] W. Hollik, J. I. Illana, S. Rigolin, C. Schappacher, and D. Stockinger, Top dipole form factors and loop-induced *CP* violation in supersymmetry, *Nucl. Phys. B* **551** (1999) 3.
- [14] M. Nowakowski, E. A. Paschos, and J. M. Rodriguez, All electromagnetic form factors, *Eur. J. Phys.* **26** (2005) 545.